Applied Geochemistry 66 (2016) 210–218

Contents lists available at ScienceDirect

Applied Geochemistry

journal homepage: www.elsevier.com/locate/apgeochem

Evidence of technetium and iodine release from a sodalite-bearing ceramic waste form

James J. Neeway [a, *], Nikolla P. Qafoku [a], Benjamin D. Williams [a], Michelle M.V. Snyder [a], Christopher F. Brown [a], Eric M. Pierce [b]

[a] Pacific Northwest National Laboratory, Richland, WA 99352, USA
[b] Oak Ridge National Laboratory, Oak Ridge, TN, USA

ARTICLE INFO

Article history:
Received 28 September 2015
Received in revised form
23 December 2015
Accepted 28 December 2015
Available online 31 December 2015

Keywords:
Technetium
Radioactive waste form
Mineral dissolution
Sodalite

ABSTRACT

Sodalites have been proposed as a possible host of certain radioactive species, specifically ^{99}Tc and ^{129}I, which may be encapsulated into the cage structure of the mineral. To demonstrate the ability of this framework silicate mineral to encapsulate and immobilize ^{99}Tc and ^{129}I, single-pass flow-through (SPFT) tests were conducted on a sodalite-bearing multi-phase ceramic waste form produced through a steam reforming process. Two samples made using a steam reformer samples were produced using non-radioactive I and Re (as a surrogate for Tc), while a third sample was produced using actual radioactive tank waste containing Tc and added Re. One of the non-radioactive samples was produced with an engineering-scale steam reformer while the other non-radioactive sample and the radioactive sample were produced using a bench-scale steam reformer. For all three steam reformer products, the similar steady-state dilute-solution release rates for Re, I, and Tc at pH (25 °C) = 9 and 40 °C were measured. However, it was found that the Re, I, and Tc releases were equal or up to 4.5x higher compared to the release rates of the network-forming elements, Na, Al, and Si. The similar releases of Re and Tc in the SPFT test, and the similar time-dependent shapes of the release curves for samples containing I, suggest that Re, Tc, and I partition to the sodalite minerals during the steam reforming process.

1. Introduction

Multi-phase ceramics are candidate materials for use as nuclear waste forms and have, therefore, been extensively studied as host matrices for radionuclides (Lumpkin, 2006). Examples of multi-phase ceramics include SYNROC ("synthetic rock") (Ringwood et al., 1978; Vance, 2012), pyrochlore (Icenhower et al., 2006; Zhang et al., 2013), pollucites (Xu et al., 2001, 2015), glass ceramics (Crum et al., 2012) and the fluidized bed steam reforming (FBSR) product (Jantzen, 2006; Neeway et al., 2012). The FBSR process has been demonstrated commercially to treat both liquid and solid low-level radioactive waste streams (Mason et al., 2003). The moderate temperature of the FBSR process (650 °C–800 °C) enables bonding of radionuclides and contaminants of concern (COCs) that would otherwise be volatile at vitrification temperatures (~1150 °C). The FBSR technology generates a granular product that is composed of sparingly soluble sodium aluminosilicate minerals, principally feldspathoids. One of the feldspathoid minerals is sodalite, which can sequester the major radionuclides ^{99}Tc (2.1×10^5 a) and ^{129}I (1.6×10^7 a) in large cavities, or β-cages, present in the network (Fig. 1). Because safe storage of nuclear waste forms relies on understanding their durability upon contact with an aqueous fluid, we have performed a set of dilute-solution experiments on the FBSR mineral product.

The FBSR product is primarily nepheline (ideally $NaAlSiO_4$) and a similar polymorph, anion-bearing sodalite [ideally $M_8[AlSiO_4]_6X_2$, where M = a 1 + cation (e.g. Na^+, Cs^+, K^+) and X = a 1- anion (e.g. Cl^-, Br^-, OH^-)], as well as a significant amorphous fraction (Williams et al., 2016). The crystalline minerals are mostly members of the feldspathoid group that contains minerals with a 1:1:1 Na:Al:Si molar ratio. Feldspathoid minerals are comprised of a three-dimensional, oxygen-tetrahedral framework with Na and Si in a network system containing multiple channels, cages, and pores (Deer et al., 2004). In terms of its role in radionuclide retention, sodalite, which can be produced by heating synthetic nepheline with NaCl (Deer et al., 2004), is the most important of the

* Corresponding author.
E-mail address: James.Neeway@pnnl.gov (J.J. Neeway).

http://dx.doi.org/10.1016/j.apgeochem.2015.12.017
0883-2927/

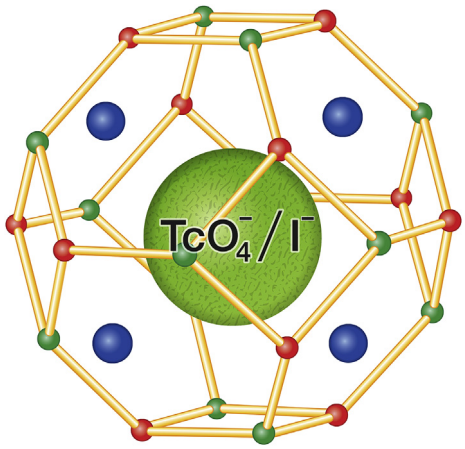

Fig. 1. Schematic showing the β-cage structure of sodalite.

feldspathoid mineral group. Sodalite cages, which result from alternating SiO_4 and AlO_4 corner-sharing tetrahedral, contain an anion at the center (Cl^- in the sodalite mineral of the sodalite group) with four tetrahedrally-associated cations (Na^+ in the sodalite mineral of the sodalite group). However, the chloride ion may be substituted with other monovalent or divalent anions, such as OH^- (basic sodalite), so_4^{2-} (nosean), and co_3^{2-} (natrodavyne), and the sodium ions may be substituted with 1 + or 2 + cations (Brenchley and Weller, 1994; Lepry et al., 2013). This flexibility allows for the direct incorporation of ReO_4^- (Dickson et al., 2014, 2015; Mattigod et al., 2006; Pierce et al., 2014) and presumably TcO_4^- (Jantzen et al., 2013) into sodalite. However, only Re has been shown to be present in the sodalite cage, first by Rietveld refinement of X-ray diffraction (XRD) patterns (Dickson et al., 2014; Mattigod et al., 2006), and more recently, through extended X-ray absorption fine structure (EXAFS) data (Dickson et al., 2015; Pierce et al., 2014).

In this study, we present results obtained from dynamic single-pass flow-through (SPFT) tests conducted on three different granular FBSR products obtained with the following waste streams and FBSR assemblies: (1) a non-radioactive low-activity waste (LAW) stream simulant and an engineering-scale assembly, (2) a non-radioactive LAW stream simulant and a bench-scale assembly, and (3) a radioactive LAW and a bench-scale assembly. The dilute-condition dissolution rates of these products can be compared to ensure that each system generates a similar product. The quantitative results, when combined with results obtained through other test methods, can then be used as input values to performance assessment models that describe the long-term impacts on public health and environmental resources of disposing of the FBSR waste form in a facility. Previous tests that have been performed on similar FBSR products are the static product consistency test (PCT) (Williams et al., 2016) and the pressurized unsaturated flow (PUF) test, which simulate dissolution in a water-unsaturated environment (Neeway et al., 2014; Pierce et al., 2014). Previously, similar SPFT tests have been run on FBSR products (Jantzen et al., 2007; Lorier et al., 2005; McGrail et al., 2003) and glass-bonded sodalite (Jeong et al., 2002; Morss et al., 2000); however, these studies were run on samples that did not contain Tc, and the systems were not run long enough to achieve a steady-state release of species from the products. Other groups have also performed dissolution studies on pure nepheline (Hamilton et al., 2001; Tole et al., 1986) and sodalite minerals (Maddrell et al., 2014), but no comparisons have been made due to their use of static dissolution conditions, as well as variable pH and temperature.

2. Methods

2.1. Production and preparation of FBSR materials

Production of the granular FBSR material uses kaolin clay, an aqueous waste stream, and a heat source, such as carbon, as the initial reactants. The granular FBSR product is formed when kaolin clay is heated and the destabilization of the clay leaves an unstable Al site, which reacts with alkali elements (i.e., Na, K, and Cs) to form new mineral phases (Jantzen, 2008), resulting in the formation of sodium aluminosilicates (NAS) and other solids. During mineralization in the presence of superheated steam and the carbon reductant, any organic matter in the aqueous waste is converted to carbon dioxide gas while nitrates and nitrites in the waste are converted to nitrogen gas. The specific reduction reactions are provided in Olson et al. (2004). Further information on the process and engineering involved in production are provided elsewhere (Neeway et al., 2012; Olson et al., 2004).

The granular products used in this set of experiments were produced at two different facilities. The first material was produced at the Hazen Research facility in Golden, Colorado, USA using the Engineering Scale Technology Demonstration (ESTD) pilot plant (TTT, 2009). The waste stream used was non-radioactive Hanford LAW simulant based on the Rassat 168 Hanford Tank Blend simulant (Lorier et al., 2005; Rassat et al., 2003). The resulting material was from the US Department of Energy (DOE) Advanced Remediation Technologies (ART) P1-B campaign; the granular material is herein referred to as P1BG, with the "G" being used to identify the granular product. The second granular material, referred to as BSRG, was created using a chemical shim of radioactive Savannah River Site (SRS) LAW (Tank 50) aqueous waste that resembles Hanford LAW. The BSRG material was produced at Savannah River National Laboratory (SRNL) using their bench-scale reformer (BSR). Results have shown that the same mineral phases were identified in the engineering-scale and bench-scale reformers (Crawford and Jantzen, 2011; Jantzen et al., 2013). The third material was produced using the SRNL BSR using feed from actual radioactive Hanford waste (Tank SX-105) and is referred to as LAW1. More details on the processing of this material, also known as Module C, is found in a report by Jantzen et al. (2013) Further information on mineralogical studies conducted with the P1BG and BSRG materials is provided elsewhere (Jantzen et al., 2013; Williams et al., 2016).

2.2. Sample composition and preparation

The concentration of each element relative to the wet mass of the sample, designated by C_0 (Table 1). The concentration of each element relative to the wet mass of the sample was analyzed using a microwave digestion technique. A mixed acid dissolution consisting of 9 mL of concentrated HNO_3 and 3 mL of concentrated HCl were added to 0.1 g of the solid sample and the mixture was microwave digested for 30 min at 210 °C. The sample was then cooled and 10 mL of a 5% boric acid and 1 mL concentrated HF was added to each vessel. The resulting mixture was then heated to 180 °C for 25 min. An aliquot of the solution was analyzed using inductively coupled plasma-mass spectroscopy (ICP-MS) and inductively coupled plasma-optical emission spectroscopy (ICP-OES) and the concentration of all elements was determined in reference to the wet mass of the sample.

Preparation of the three granular FBSR materials involved sieving the received sample and washing with absolute ethanol to remove adhering fines. This step occurred while the product was still on the sieves. Acid digestion data indicate that there was no change in the product composition as a result of the ethanol wash. The material was dried and placed in a muffle furnace at 525 °C for

Table 1
Composition of major elements in the FBSR samples used in this study in mass percent. Compositions were determined from an acid digestion of the solids. Concentrations of the different species were measured with the listed analytical methods.

	P1BG[a]	BSRG[b]	LAW1 (SX-105)[c]	Analytical method
Al_2O_3	31.74	32.50	32.50	ICP-OES
Na_2O	19.01	19.55	19.14	ICP-OES
SiO_2	38.51	38.94[d]	40.43[d]	ICP-OES
ReO_2	0.02	0.04	0.02	ICP-MS
TcO_2	NI	NI	5.2E-04	ICP-MS
I	0.06	0.07	8.7E-04[d]	ICP-MS
Cs_2O	0.14	0.30	1.1E-03[d]	ICP-MS
SO_4[d]	1.29	1.08	0.67	IC
PbO	0.23	0.11	0.13	ICP-MS
Fe_2O_3	2.43	1.43	1.72	ICP-OES
Cr_2O_3	0.12	0.09	0.12	ICP-OES
BaO	0.17	0.02	–	ICP-OES
Moisture Content	0.35	0.31[d]	1.32	
Coal	1.31	1.12[d]		
Sum	95.37	95.54	96.05	

NI = not included.
[a] Granular Rassat LAW Tank Blend from ESTD.
[b] Granular Rassat LAW Tank Blend from BSR.
[c] Granular radioactive LAW from tank SX-105.
[d] Value from (Jantzen et al., 2013).

2 h to remove any residual carbon (coal) remaining from production. The P1BG material was sieved to a +325–100 mesh (44–149 μm) size fraction. The BSRG sample was sieved to a +200–100 mesh (74–149 μm) size fraction. The difference in size fraction between the two samples was a result of the fine-grained nature of the P1BG material, which consisted of 80 mass% of material from the high-temperature filter, and thus necessitated a smaller size fraction be chosen for dissolution testing. Finally, the LAW1 (SX-105) granular sample made in the SRNL BSR was composed of a +100 mesh (149 μm) size fraction. Again, the choice of size fraction depended on the limited amount of sample.

2.3. Experimental solution compositions

All solutions were buffered at pH 9 using a solution of 0.05 *M tris (hydroxymethyl) aminomethane* (THAM), which was adjusted to the desired pH using high-purity 15.8 M HNO_3. Solution pHs were measured at room temperature. The pH values were monitored throughout the test at the inlet and effluent solutions. The precision of the pH measurements was ±0.02 pH units. The pH values were checked against buffer standards of 4, 7, and 10 (Fisher), and then checked with another set of buffers (ERA) to ensure accuracy. In a series of measurements, the buffer at pH 7 was re-measured after every 10 effluent solutions to ensure there was no drift in the electrode.

2.4. Single-pass flow-through dissolution experiments

Dissolution experiments were conducted using the SPFT method (ASTM, 2010). A schematic apparatus of the SPFT system is presented in Fig. 2. The SPFT system is designed to have a continuous flow of fresh solution into a reactor containing the material of interest. When the ratio of the solution flow rate to the sample surface area is large enough, species leached into solution from the product will not reach saturation with respect to possible secondary phase formation and the far-from-equilibrium dissolution rate of the material can be measured. The system uses syringe pumps (Kloehn, Las Vegas, NV, USA) that draw the buffered solution from the input reservoirs and transfer it to the reactor vessels through Teflon tubing. The Teflon tubing is inserted into a 60-mL Teflon

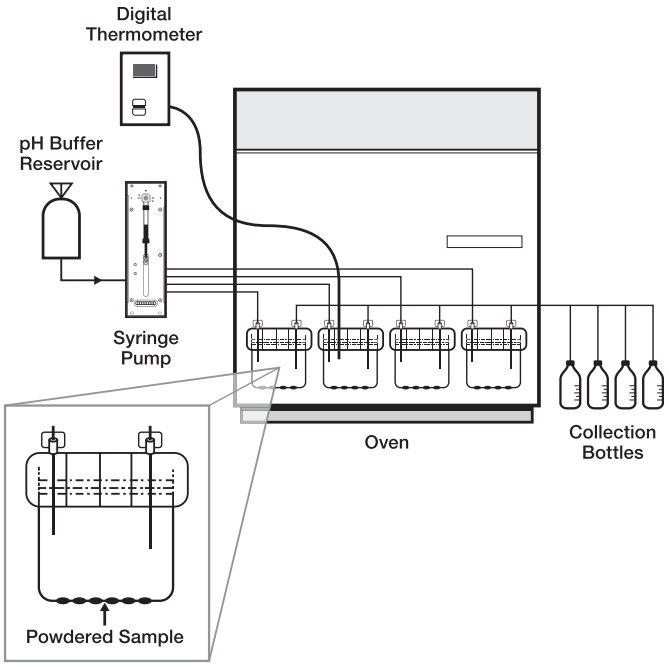

Fig. 2. Schematic of the single-pass flow-through (SPFT) apparatus for determining reaction rates in continuous-flow solution.

reactor containing the granular FBSR solid sample at the bottom of the reactor in a thinly dispersed layer. Solution flows from the reactor through an outlet port on the lid of the Teflon reactor.

The input reservoirs were maintained at 40 ± 2 °C to ensure a stable solution temperature, even at high flow rates. Flow rates were determined from gravimetric analysis of the effluent container at defined sampling periods. Variations in flow rates over the duration of the tests were within 10% of the target flow rate. In the few cases where a flow rate did drop due to mechanical failures in the system, the system was repaired and the flow rate was reset within a period of one day. The SPFT system design ensures adequate mixing of the solids with influent. All influent and effluent solutions were analyzed for Al, Na, and Si with ICP-OES and for Re, I, Cs, Tc, and Cr with ICP-MS. For some of the samples, the elemental concentrations were below the estimated quantification limit (EQL), which is defined by the lowest calibration standard that can be reproducibly determined during an analytical run within 10% of the certified value multiplied by the sample dilution factor. The anions SO_4^{2-}, PO_4^{3-}, NO_3^-, and NO_2^- were monitored using ion chromatography; however, the anion concentrations were always below the mean detection limit after the first few sampling events, and therefore are not reported in this paper. Experimental conditions, dissolution rates, and experimental uncertainties for all of the tests are given in Table 2. The measured concentrations of several elements of concern are given in the Supplementary Materials.

2.5. Dissolution rates and error

A general dissolution model, based on Transition State Theory, is given by the general equation (Eq. (1)):

$$r = \nu_i k a_{H^+}^{-\eta} \exp\left(\frac{-E_a}{RT}\right)\left[1 - \left(\frac{Q}{K_g}\right)\right] \quad (1)$$

where r is the dissolution rate (g m^{-2} d^{-1}), ν_i is the stoichiometric coefficient of element i in the glass, k is the intrinsic rate constant (g m^{-2} d^{-1}), a is the hydrogen ion activity, E_a is the activation

Table 2
Experimental run conditions for experiments at 40 °C and pH 9. Values in parentheses represent the standard deviation (σ) of the average *q/S* value throughout the experiment.

Sample ID	BET specific surface area (m^2/g)	Mass (g)	Average flow rate (mL/d)	*q/S* (10^{-5} × m/d)	Duration (days)
P1BG	5.7	0.25	298	20.8 (3.3)	56.0
		0.25	198	13.8 (2.2)	56.0
		0.50	149	5.20 (0.82)	56.0
		0.75	90.0	2.10 (0.33)	63.0
		0.75	5.64	1.14 (0.18)	63.0
		1.00	10.1	0.18 (0.03)	63.0
BSRG	3.6	0.25	304	33.8 (5.3)	28.0
		0.25	208	23.1 (3.7)	28.0
		0.50	159	8.81 (1.39)	28.0
		0.75	91.0	3.37 (0.53)	39.8
		0.76	53.0	1.94 (0.31)	39.7
		0.99	14.2	0.40 (0.06)	73.9
LAW1	3.6	0.25	286	31.9 (5.1)	58.0
		0.51	146	8.08 (1.28)	58.0
		1.07	10.4	0.27 (0.04)	58.0

energy (kJ/mol), R is the gas constant (kJ/mol·K), T is the temperature (K), Q is the ion activity product, K_g is the pseudoequilibrium constant, η is the pH power law coefficient, and it is assumed that H^+ is the only aqueous species that can directly influence the rate. Quantification of parameters can be achieved by changing experimental conditions, such as temperature, flow rate, pH, and the concentration of certain aqueous species. If we assume a constant temperature and pH, Eq. (1) simplifies to (Eq. (2)).

$$r = k\left[1 - \frac{Q}{K}\right] \tag{2}$$

Therefore, by running the experiments in dilute conditions, Q approaches zero and the rate of mineral dissolution is equal to the temperature- and pH-dependent intrinsic rate constant, k.

The rate, r, from Eq. (2) can be calculated from the normalized release rate of element i per unit area of glass (g m^{-2} d^{-1}) (Eq. (3)):

$$r_i = \frac{(c_i^{out} - c_i^{in}) \cdot q}{f_i \cdot S} \tag{3}$$

where r_i is the normalized release rate, c_i^{out} is the concentration of element i in the effluent (g m^{-3}), c_i^{in} is the elemental concentration of the influent (g m^{-3}), q is the flow rate (m^3 s^{-1}), f_i is the mass fraction of the element in the original material (dimensionless), and S is the surface area of the sample (m^2). In all cases, the background analyte was below the detection limit for the blank using the given analytical method, and the mean limit of detection was used as the concentration of the element in the influent for calculations. The steady-state at each flow rate was determined when three subsequent effluent samples had concentrations of the analyte of interest that differed by less than 10% from one another. These conditions were usually obtained after three weeks of reaction time. When applying this method to the multi-phase FBSR product, we acknowledge that the rates calculated from a given element are the sum of the release rates of the element from each individual phase of the material.

3. Results

3.1. Temporal concentration profiles

3.1.1. Non-radioactive engineering-scale product (P1BG)

The normalized concentration (NC_i where i = Na, Al, Si, Cs, Re, or I) from experiments conducted with the P1BG material at flow rates of 300, 150, and 10 mL/d are given in Fig. 3. We begin with a discussion of the release behavior of the major elements, Na, Si, and Al. The data at the various flow rates indicate that, at short time periods, the release of Na is about an order of magnitude larger than the releases of Si and Al. For instance, at longer time periods and for flow rates greater than 90 mL/d (not shown), the concentration of Na, Al, and Si converge. However, for rates less than 90 mL/d, the long-term NC_{Na} remains higher than the others. At the lowest flow rate (10 mL/d), the NC_{Na} stays higher than that of Si and Al by a factor of three after two months of testing. In general, it is also observed that the NC_{Na} decreases sharply after the first few samplings and then approaches NC_{Al} and NC_{Si}. For the lower flow rates, the Na concentration stays constant for a few samplings and then decreases slowly, but never approaches that of Si and Al.

For Al and Si, the two elements seem to be released concomitantly at all flow rates. The NC_{Al} and NC_{Si} for the first sampling stay roughly the same across all flow rates (~1×10^3 μmol/L). Thereafter, Al and Si demonstrate similar release curves. At the higher flow rates, NC_{Na}, NC_{Al} and NC_{Si} decrease after about 30 days, suggesting that the surface area available for dissolution is decreasing with time. In the subsequent section, release rates are calculated using elemental concentrations obtained at three to four weeks of testing in order to avoid inaccurate corrections to the material surface area.

Fig. 3 also shows the releases of Cs, I, and Re as a function of time at each flow rate for P1BG. The graphs show that Re and I follow similar trends, whereas Cs follows trends more similar to Na, Al, and Si. This is because Cs^+ can be substituted for Na^+ in the feldspathoid structure, albeit with an assumed expansion of the mineral structure to accommodate the larger cation (Lepry et al., 2013). Despite this expected substitution, the apparent increase in Cs concentration for the lower flow rates indicates that Cs may also be present elsewhere in the FBSR waste form. On the other hand, the release of Re and I in the granular material seems delayed with respect to the bulk sodium aluminosilicate product. We observe an initial high release, which then drops and subsequently rises through a second maximum as the time progresses. For rate calculations given in a Section 3.2, the concentration of these two elements at the second maximum is defined as the steady-state concentration. This definition is considered conservative. It should be noted that this time frame was also chosen for calculations of the forward dissolution rate based on Na, Al, and Si releases.

Additionally, the concentration of the SO_4^{2-}, another COC, was measured, but the concentration of the anion was below the instrument detection limit (1.5 μg mL^{-1}) after approximately three reactor volumes. Therefore, no conclusive results are available for the release of this anion. Other COCs, such as Ba and Pb, were below

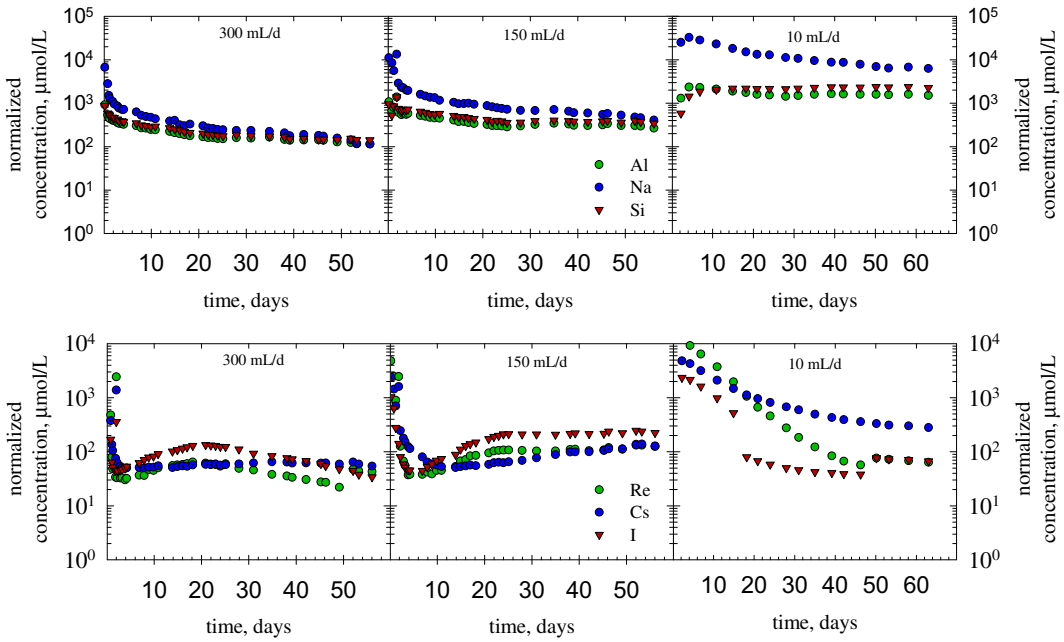

Fig. 3. P1BG normalized concentrations (µmol/L) versus time of Al, Na, and Si (top) and Re, Cs, and I (bottom) for SPFT tests run at 40 °C either at a solution flow rate of 300 mL/d (left), 150 mL/d (center), or 10 mL/d (right). Note the change in scale for the y-axis between the two graphs.

quantifiable limits at the higher flow rates. This is the case for the BSRG and LAW1 (SX-105) products as well.

3.1.2. Non-radioactive bench-scale product (BSRG)

The concentrations of Na, Al, and Si for the BSRG material follow similar trends to the P1B material. Graphs of NC_i versus time are presented in Fig. 4. The only noticeable difference between the results from the BSRG and P1BG materials is that release concentrations stay constant for the entire testing period for BSRG whereas the P1BG material seems to show decreases in elemental concentrations at high flow rates and long time periods, most likely due to a diminishing surface area. It is unclear if the BSRG materials would behave similarly if the experimental duration for this material was longer than one month.

Releases of Cs, I, and Re from the BSRG product are also presented in Fig. 4. We observe a similar trend to the P1B product where NC_{Cs} does not decrease to a similar extent as I and Re values at short time periods. Again this may be indicating that Cs is substituting for Na in the framework mineral. Also, as with P1B, we observe an increase in release concentrations for I and Re after the

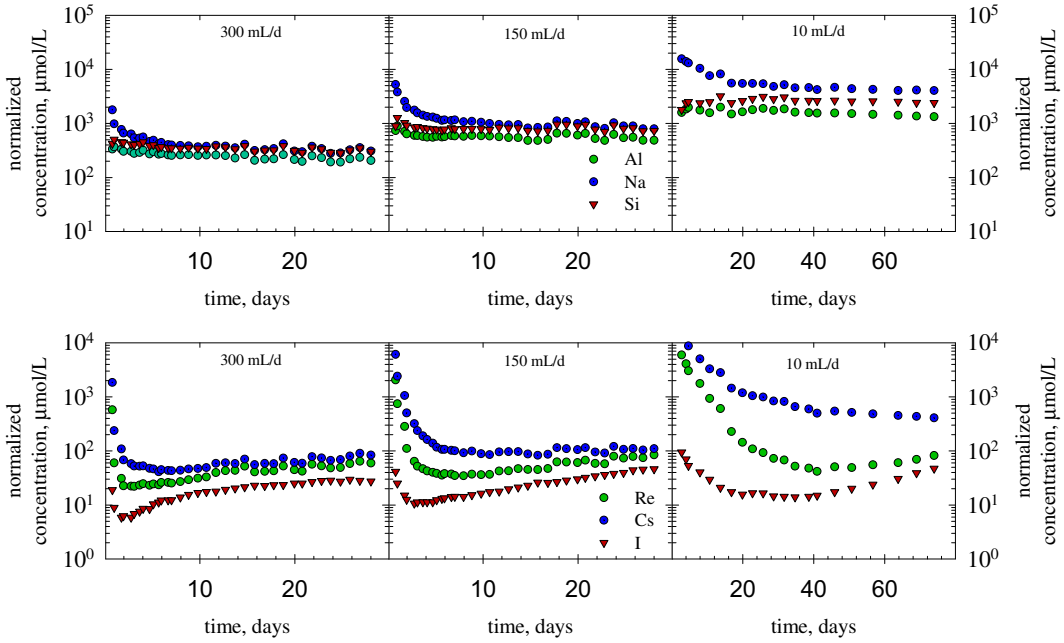

Fig. 4. BSRG normalized concentrations (µmol/L) versus time of Al, Na, and Si (top) and Re, Cs, and I (bottom) for SPFT tests run at 40 °C either at a solution flow rate of 300 mL/d (left), 150 mL/d (center), or 10 mL/d (right).). Note the change in scale for the y-axis between the two graphs.

initial drop at short time periods. However, for this set of experiments, we do not see NC_i reach a second maximum before dropping again. This, again, may be due to the shorter experimental duration for the study with BSRG.

3.1.3. Radioactive bench-scale product (LAW1)

Values of NC_{Na}, NC_{Al} and NC_{Si} from the LAW1 material are given in Fig. 5. In general, similar conclusions can be drawn from this material as those found for the other granular FBSR products, P1BG and BSRG. The only major difference is that, for the high flow rate sample, the short-term release of Na is more consistent with the releases of Si and Al observed in the P1BG and BSRG samples. This may be due to the absence of unreacted Na in the final product material.

The temporal release of Cs, Re, I, Tc, and Cr have also been followed throughout the SPFT tests for the LAW1 material. Because of the relatively low concentrations of Cs and I in the starting materials, these two elements were consistently below the EQL of 0.06 ppb and 0.5 ppb for Cs and I, respectively, and so their values are not presented here. On the other hand, the outlet concentration of the Cr was followed throughout because of the relatively high concentration of this COC in the starting material. The results for the release of Re, Cr, and Tc versus time are given in Fig. 5 for the LAW1 material. The results show that the release of Tc and Re are concomitant, suggesting they may be released from the same mineral phase. The LAW1 material differs from the P1BG and BSRG material in that there is not a sharp decrease in NC_{Tc} and NC_{Re} at short time periods. This observation would suggest that only small amounts of perrhenate or pertechnetate salts are produced during fabrication, and that Re and Tc releases are most likely controlled by sodalite dissolution rates. The release of Cr does not show the pattern of a decrease, increase, and subsequent decrease in release concentrations versus time as has been observed for Re, I, and now Tc for the various materials. This is consistent with SEM/EDS observations of the material showing that Cr exists as a separate Cr phase, which has previously been identified as a spinel phase (Jantzen et al., 2013).

3.2. Kinetics of material dissolution

The SPFT method is commonly used in the geochemistry community, where it has been employed to measure reaction rates of both minerals (Dove and Crerar, 1990; Gudbrandsson et al., 2014; Hamilton et al., 2000; Oelkers et al., 2008) and glasses (Icenhower et al., 2008, Icenhower and Steefel, 2013; McGrail et al., 1997; McGrail et al., 2001; Neeway et al., 2011; Pierce et al., 2005, 2008, 2010). The method involves running leach tests at several q/S, or flow-rate-to-surface-area, values. Once a high enough q/S value is reached, the measured release rate of an element used as a dissolution tracer no longer changes with increasing q/S values. This indicates that the solution is unsaturated with respect to secondary phase formation and that the release of the tracer elements comes only from the mineral or glass of interest. Though our SPFT tests that were run for periods of up to two months, the steady-state release concentration was often achieved in approximately three weeks of experiment; though, at the lowest flow rates, steady-state concentrations were achieved on the order of four weeks of experiment.

The resulting curves from all three studied materials for Si, Na, and Al release rates as a function of q/S are presented in Fig. 6. From the figure, it is seen that a release rate independence of the flow rate for Al and Si occurs when the flow rate is at 200 mL d^{-1} and above (i.e., the two points for each material farthest to the right on the q/S curves). Though an argument may be made that the rate measured at 150 mL/d for these materials may be equal to the higher flow rates within a 2σ uncertainty, a decision has been made not to include results from this flow rate in the calculation of forward dissolution rates. This decision was made because, for some materials, the q/S value at 150 mL d^{-1} decreases slightly compared to results obtained at 200 and 300 mL d^{-1}. We note that one previous experiment chose 150 mL d^{-1} to create a dilute solution (McGrail et al., 2003) while a later test chose 200 mL d^{-1} (Lorier et al., 2005). For Na, a significant contribution from a Na source gives rates that do not decrease significantly at the lower flow rates (i.e., to the left on the q/S graph).

The values of NC_{Cs}, NC_I, NC_{Re}, and NC_{Tc} as a function of q/S are

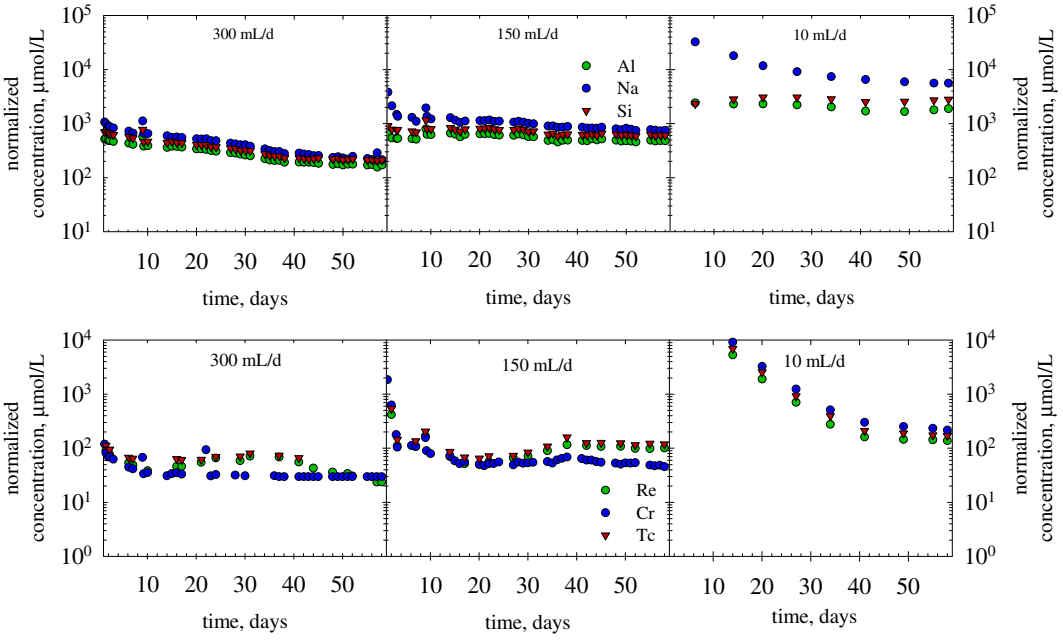

Fig. 5. Normalized concentrations versus time of Al, Na, and Si (top) and Re, Cr, Tc (bottom) for the LAW1 (SX-105) material.

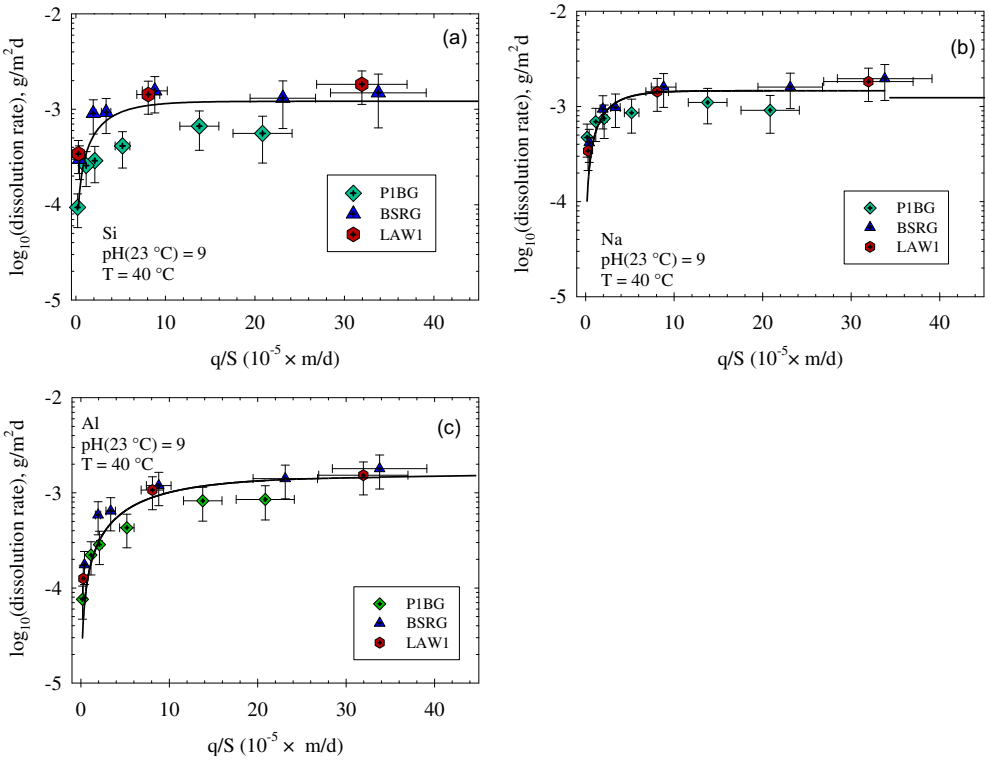

Fig. 6. Release rates (g m^{-2} d^{-1}) as a function of the ratio of the flow rate (q) to the sample surface (S) for (a) Si, (b) Na, and (c) Al. The data were regressed using an equation of the form $y = a(1-e^{-xb})$. The resulting line is used to lead the eye.

presented in Fig. 7. The values of NC_I, and NC_{Re}, are higher at the higher flow rates and are up to three orders of magnitude higher than release rates observed at the lower flow rates. Though one would expect rates to be lower at the lower flow rates because of

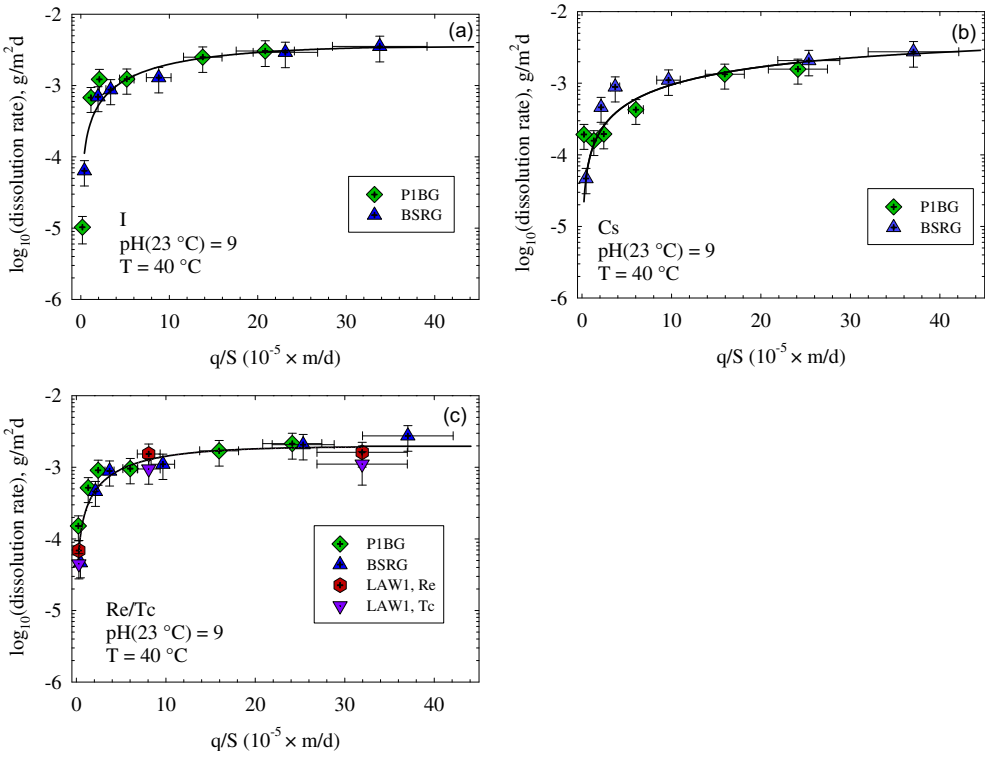

Fig. 7. Release rates (g m^{-2} d^{-1}) as a function of the ratio of the flow rate (q) to the sample surface (S) for (a) I, (b) Cs, and (c) Re/Tc. The data were regressed through an equation of the form $y = a(1-e^{-xb})$. The resulting line is used to lead the eye.

the buildup of constituents in the contacting solution, this difference in releases, compared to similar ratios seen for the NAS backbone, seems quite high. An explanation for this is most likely that the steady-state concentration used to calculate the rates in our SPFT tests is an underestimation resulting from experiments that were too short in duration to observe the delayed growth in Re and I releases observed at the higher flow rates.

Lastly, from the collected data for P1BG, BSRG, and LAW1, forward release rates were performed from flow rates at 200 and 300 mL d^{-1}. For P1BG and BSRG, the releases of Re and I are double those seen from the other measured elements (i.e., Na, Al, Si, Cs). This is not the case for Re and Tc release rates from the LAW1 product, which shows release rates similar to Na, Al, and Si from the radioactive waste form.

4. Discussion

A summary of the elemental release rates is provided in Table 3, where they are compared to the study of another FBSR product by Lorier et al. (2005). A minor difference in the elemental release rate of Re was found when comparing the two studies. This difference may be explained by our hypothesis that Lorier et al. (2005) ran their SPFT tests for an insufficient time period to allow adequate growth of the Re signal from the delayed release of anions from the sodalite phase. Sulfur release rates, from ICP-OES measurements from the Lorier et al. (2005) study, are double those observed from the Re release. It would not be expected for S and Re (as well as Tc and I, by extension) to have different release rates because they are all in the sodalite cages; therefore, the large error (2σ) in the Lorier et al. (2005) sulfur data set may be masking the actual behavior of S. Despite slight discrepancies between the two studies, these values are one order of magnitude lower than the forward dissolution rates of LAW boroaluminosilicate and borosilicate glasses measured at the same pH and temperature. (Icenhower et al., 2008) Therefore, we suggest that the granular FBSR products used in this study would make a comparable waste form to glass after the granular FBSR product is bound into a monolith.

Results given in this study can be compared to similar tests performed on FBSR materials that have been performed previously. McGrail et al. (2003) observed a similar delay in the release of S and Re from a similar steam reformer product known as SCT02-098, a product of an engineering study using the THOR© steam reforming technology (McGrail et al., 2003). The authors suggest that the initial low rates earlier in the experiment were the result of being saturated with respect to a sodalite phase [nosean ($Na_8(AlSiO_4)_6(SO_4)$)] at short time periods. However, their modeling results indicated that they were far below saturation with respect to nosean. McGrail et al. (2003) did not report data for I release, and the studies were only conducted for 24 days, which did not allow the observation of sodalite dissolution increasing and then slowing at long time periods for the higher flow rates. The study by Lorier et al. (2005) presents data from experiments conducted for only 14 days and no I release data was given. Therefore, we conclude that this is the first demonstration to show that Re and I have similar release behavior, and that similar behavior of Re and Tc also occurs if those elements are assumed to be present in the same mineral phase. The release of I, Re, and Tc is assumed to be from the sodalite cage, which has been proposed as a getter in nuclear waste immobilization.

Table 3
Release rates (10^{-4} × g m^{-2} d^{-1}) for elements from this study run at 40 °C and buffered at pH(25 °C) 9.

Element	P1BG	BSRG	LAW1 (SX-105)
Al	8 ± 2	16 ± 4	15 ± 6
Na	10 ± 3	18 ± 5	18 ± 7
Si	6 ± 2	14 ± 5	16 ± 6
Re	19 ± 5	24 ± 6	16 ± 6
I	28 ± 8	32 ± 8	NA
Cs	28 ± 8	7.5 ± 2	NA
S	NA	NA	NA
Tc	NA	NA	11 ± 5

FBSR offers a continuous method by which Hanford LAW can be processed into a crystalline mineral waste form at moderate temperatures (725–750 °C). The resulting material is multi-phase and consists primarily of nepheline, with some nosean and sodalite also present. In this study, a non-radioactive granular material produced at the engineering scale, and radioactive and non-radioactive materials produced at the bench scale, were studied. The forward dissolution rate of the various FBSR products in an infinitely dilute solution concentration with respect to secondary phases were calculated at pH 9 and 40 °C. When measuring the dissolution rates of the materials, it is difficult to separate the contribution of various mineral phases in the FBSR product and the calculated release rate will be controlled by the mineral with the fastest dissolution rate. When examining the release of the various species as a function of time, the release of I, Re, and Tc have a different shape than Al, Na, Cs and Si, indicating that the release of these elements is controlled by a phase that has a different solubility compared with the bulk NAS phase. We assume that this different phase is sodalite. Sodalite has been previously shown to incorporate Re into the structure and, because the FBSR process has been shown to produce sodalite, Re, I, and Tc are presumed to be leached from this phase. The delayed release of elements from the sodalite phase compared to the bulk NAS phase indicates either that the bulk NAS phase must dissolve first in order to access sodalite crystals or the two phases have largely different release kinetics.

The release rates calculated using elements contained in the materials are near 1×10^{-3} g m^{-2} d^{-1}. In comparison, tests on the P1BG granular material conducted in unsaturated moisture, non-dilute leachant conditions showed the release of all the studied elements were dissimilar; I and Re were shown to be released at a rate roughly 100 × faster (~10^{-4} g m^{-2} d^{-1}) than the relatively insoluble Si (~10^{-6} g m^{-2} d^{-1}) when the experiment had reached a steady state. (Neeway et al., 2014) It should be noted that all the rates calculated from this set of experiments used a specific surface area determined using N_2 adsorption/desorption isotherms, which may be a slight overestimate of the actual surface area and thus underestimate the dissolution rate of the material. However, even using a non-conservative geometric surface area, the rates are similar to those calculated for a LAW glass. Therefore, the FBSR process may be a viable method of supplemental waste treatment to aid in meeting the Hanford site cleanup schedule.

Acknowledgments

These studies were supported by the U.S. Department of Energy (DOE) through the Office of Environmental Management. Pacific Northwest National Laboratory (PNNL) is operated for the DOE by Battelle Memorial Institute under Contract DE-AC06-76RLO 1830. We would like to recognize our PNNL colleagues Elsa Cordova, Sara Strandquist, DeNomy Dage, Jesse Lang, Michael Schweiger, and Cristian Iovin for the contributions to the tests used in this study, as well as the Savannah River National Laboratory (SRNL) team who prepared the samples, including Carol Jantzen, Charles Crawford, Christopher Bannochie, Paul Burket, Alex Cozzi, Gene Daniel, Connie Herman, Charles Nash, Donald Miller, and Holly Hall. We would also like to thank R. Jeffrey Serne of PNNL and Carol Jantzen of SRNL for their helpful comments to greatly improve the quality of this

paper. Heather Culley (PNNL) provided technical editing of this document.

Appendix A. Supplementary data

Supplementary data related to this article can be found at http://dx.doi.org/10.1016/j.apgeochem.2015.12.017.

References

ASTM, 2010. Standard practice for measurement of the glass dissolution rate using the single-pass flow-through test method. ASTM C1662-10. ASTM International, West Conshohocken, PA.

Brenchley, M.E., Weller, M.T., 1994. Synthesis and structures of $M_8[ALSiO_4]_6\cdot(XO_4)_2$, m = Na, Li, K; x = Cl, Mn sodalites. Zeolites 14, 682–686.

Crawford, C.L., Jantzen, C.M., 2011. Evaluation of THOR™ Mineralized Waste Forms (Granular and Monolith) for the DOE Advanced Remediation Technologies (ART) Phase 2 Project. SRNL-STI-2009–00505. Savannah River National Laboratory, Aiken, SC, USA.

Crum, J.V., Turo, L., Riley, B., Tang, M., Kossoy, A., 2012. Multi-phase glass-ceramics as a waste form for combined fission products: alkalis, alkaline earths, lanthanides, and transition metals. J. Am. Ceram. Soc. 95, 1297–1303.

Deer, W.A., Howie, R.A., Wise, W.S., Zussman, J., 2004. Framework silicates: silica minerals, feldspathoids, and the zeolites. Rock-Forming Minerals, 4B. The Geological Society, London, U.K.

Dickson, J.O., Harsh, J.B., Flury, M., Lukens, W.W., Pierce, E.M., 2014. Competitive incorporation of perrhenate and nitrate into sodalite. Environ. Sci. Technol. 48, 12851–12857.

Dickson, J.O., Harsh, J.B., Lukens, W.W., Pierce, E.M., 2015. Perrhenate incorporation into binary mixed sodalites: the role of anion size and implications for technetium-99 sequestration. Chem. Geol. 395, 138–143.

Dove, P.M., Crerar, D.A., 1990. Kinetics of quartz dissolution in electrolyte solutions using a hydrothermal mixed flow reactor. Geochim. Cosmochim. Acta 54, 955–969.

Gudbrandsson, S., Wolff-Boenisch, D., Gislason, S.R., Oelkers, E.H., 2014. Experimental determination of plagioclase dissolution rates as a function of its composition and pH at 22 degrees C. Geochim. Cosmochim. Acta 139, 154–172.

Hamilton, J.P., Pantano, C.G., Brantley, S.L., 2000. Dissolution of albite glass and crystal. Geochim. Cosmochim. Acta 64, 2603–2615.

Hamilton, J.P., Brantley, S.L., Pantano, C.G., Criscenti, L.J., Kubicki, J.D., 2001. Dissolution of nepheline, jadeite and albite glasses: toward better models for aluminosilicate dissolution. Geochim.Cosmochim. Acta 65, 3683–3702.

Icenhower, J.P., Strachan, D.M., McGrail, B.P., Scheele, R.A., Rodriguez, E.A., Steele, J.L., Legore, V.L., 2006. Dissolution kinetics of pyrochlore ceramics for the disposition of plutonium. Am. Mineralogist 91, 39–53.

Icenhower, J.P., McGrail, B.P., Shaw, W.J., Pierce, E.M., Nachimuthu, P., Shuh, D.K., Rodriguez, E.A., Steele, J.L., 2008. Experimentally determined dissolution kinetics of Na-rich borosilicate glass at far from equilibrium conditions: Implications for transition state Theory. Geochim. Cosmochim. Acta 72, 2767–2788.

Icenhower, J.P., Steefel, C.I., 2013. Experimentally determined dissolution kinetics of SON68 glass at 90°C Over a silica saturation interval: evidence against a linear rate law. J. Nucl. Mater. 439, 137–147.

Jantzen, C., Crawford, C.L., Bannochie, C., Burket, P., Cozzi, A., Daniel, W., Hall, H., Miller, D., Missimer, D., Nash, C., Williams, M., 2013. Radioactive Demonstration of Mineralized Waste Forms Made from Hanford Low Activity Waste (Tank Farm Blend) by Fluidized Bed Steam Reformation (FBSR). SRNL-STI-2011–00383, Aiken, SC, USA.

Jantzen, C.M., 2006. Characterization and Performance of Fluidized Bed Steam Reforming (FBSR) Product as a Final Waste Form, Environmental Issues and Waste Management Technologies in the Ceramic and Nuclear Industries IX. John Wiley & Sons, Inc, pp. 319–329.

Jantzen, C.M., Lorier, T.H., Pareizs, J.M., Marra, J.C., 2007. Fluidized bed steam reformed (FBSR) Mineral waste forms: characterization and durability testing. In: Dunn, D. (Ed.), Scientific Basis for Nuclear Waste Management XXX, pp. 379–386.

Jantzen, C.M., 2008. Mineralization of Radioactive Wastes by Fluidized Bed Steam Reforming (FBSR): Comparisons to Vitreous Waste Froms and Pertinent Durability Testing. WSRC-STI-2008–00268. Savannah River National Laboratory, Aiken, SC, USA.

Jeong, S.-Y., Fanning, T.H., Morss, L.R., Ebert, W.L., 2002. Corrosion tests to determine temperature and pH dependencies of the dissolution rates of sodalite, binder glass, and ceramic waste form. ANL-02/32. Argonne National Laboratory, Argonne, IL, USA.

Lepry, W.C., Riley, B.J., Crum, J.V., Rodriguez, C.P., Pierce, D.A., 2013. Solution-based approaches for making high-density sodalite waste forms to immobilize spent electrochemical salts. J. Nucl. Mater. 442, 350–359.

Lorier, T.H., Pareizs, J.M., Jantzen, C.M., 2005. Single-pass Flow through (SPFT) Testing of Fluidized-bed Steam Reforming (FBSR) Waste Forms. WSRC-TR-2005–00124. Savannah River National Laboratory, Aiken, SC, USA.

Lumpkin, G.R., 2006. Ceramic waste forms for actinides. Elements 2, 365–372.

Maddrell, E., Gandy, A., Stennett, M., 2014. The durability of iodide sodalite. J. Nucl. Mater. 449, 168–172.

Mason, J.B., McKibbin, J., Ryan, K., Schmoker, D., 2003. Steam Reforming Technology for Denitration and Immobilization of DOE Tank Wastes. WM2003 Conference, Tucson, Arizona.

Mattigod, S.V., Peter McGrail, B., McCready, D.E., Wang, L.-Q., Parker, K.E., Young, J.S., 2006. Synthesis and structure of perrhenate sodalite. Microporous Mesoporous Mater. 91, 139–144.

McGrail, B.P., Ebert, W.L., Bakel, A.J., Peeler, D.K., 1997. Measurement of kinetic rate law parameters on a Na·Ca·Al borosilicate glass for low-activity waste. J. Nucl. Mater. 249, 175–189.

McGrail, B.P., Icenhower, J.P., Shuh, D.K., Liu, P., Darab, J.G., Baer, D.R., Thevuthasen, S., Shutthanandan, V., Engelhard, M.H., Booth, C.H., Nachimuthu, P., 2001. The structure of Na_2O-Al_2O_3-SiO_2 glass: impact on sodium ion exchange in H_2O and D_2O. J. Non-crystalline Solids 296, 10–26.

McGrail, B.P., Pierce, E.M., Schaef, H.T., Rodriguez, E.A., Steele, J.L., Owen, A.T., Wellman, D.M., 2003. Laboratory Testing of Bulk Vitrified and Steam Reformed Low-activity Waste Forms to Support a Preliminary Risk Assessment for an Integrated Disposal Facility. PNNL-14414. Pacific Northwest National Laboratory, Richland, WA, USA.

Morss, L.R., Stanley, M.L., Tatko, C.D., Ebert, W.L., 2000. Corrosion of glass-bonded sodalite as a function of pH and Temperature. In: Shoesmith, D.W., Smith, R.W. (Eds.), Scientific Basis for Nuclear Waste Management XXIII, 608. Materials Research Society, Boston, MA, USA, pp. 733–739.

Neeway, J.J., Abdelouas, A., Grambow, B., Schumacher, S., 2011. Dissolution mechanism of the SON68 reference nuclear waste glass: new data in dynamic system in silica saturation conditions. J. Nucl. Mater. 415, 31–37.

Neeway, J.J., Qafoku, N.P., Westsik Jr., J.H., Brown, C.F., Jantzen, C.M., Pierce, E.M., 2012. Radionuclide and contaminant immobilization in the fluidized bed steam reforming waste product. In: Radioactive Waste. InTech, ISBN 978-953-51-0551-0.

Neeway, J.J., Qafoku, N.P., Williams, B.D., Rod, K., Bowden, M.E., Brown, C.F., Pierce, E.M., 2014. Performance of the fluidized bed steam reforming product under hydraulically unsaturated conditions. J. Environ. Radioact. 313, 119–128.

Oelkers, E.H., Schott, J., Gauthier, J.-M., Herrero-Roncal, T., 2008. An experimental study of the dissolution mechanism and rates of muscovite. Geochim. Cosmochim. Acta 72, 4948–4961.

Olson, A.L., Soelberg, N.R., Marshall, D.W., Anderson, G.L., 2004. Fluidized Bed Steam Reforming of Hanford LAW Using THOR^{sm} Mineralizing Technology. INEEL/EXT-04–02492. Idaho National Engineering and Environmental Laboratory, Idaho Falls, ID, USA.

Pierce, E.M., Reed, L.R., Shaw, W.J., Icenhower, J.P., 2005. Effect of Al/B ratio on the dissolution of nepheline glass, $Na_3(Al, B)_{1\text{-}4}Si_4O_{16}$. Geochim. Cosmochim. Acta 69, A781.

Pierce, E.M., Richards, E.L., Davis, A.M., Reed, L.R., Rodriguez, E.A., 2008. Aluminoborosilicate waste glass dissolution under alkaline conditions at 40°C: implications for a chemical affinity-based rate equation. Environ. Chem. 5, 73–85.

Pierce, E.M., Reed, L.R., Shaw, W.J., McGrail, B.P., Icenhower, J.P., Windisch, C.F., Cordova, E.A., Broady, J., 2010. Experimental determination of the effect of the ratio of B/Al on glass dissolution along the nepheline ($NaAlSiO_4$)-malinkoite ($NaBSiO_4$) join. Geochim. Cosmochim. Acta 74, 2634–2654.

Pierce, E.M., Lukens, W.W., Fitts, J.P., Jantzen, C.M., Tang, G., 2014. Experimental determination of the speciation, partitioning, and release of perrhenate as a chemical surrogate for pertechnetate from a sodalite-bearing multiphase ceramic waste form. Appl. Geochem. 42, 47–59.

Rassat, S.D., Mahoney, L.A., Russell, R.L., Bryan, S.A., Sell, R.L., 2003. Cold Dissolved Saltcake Waste Simulant Development, Preparation, and Analysis. PNNL-14194 Rev. 1. Pacific Northwest National Laboratory, Richland, WA, USA.

Ringwood, A.E., Kesson, S.E., Ware, N.G., Hibberson, W., Major, A., 1978. Immobilization of high-level nuclear-reactor wastes in SYNROC. Nature 278, 219–223.

Tole, M.P., Lasaga, A.C., Pantano, C., White, W.B., 1986. The kinetics of dissolution of nepheline (NaAlSiO4). Geochim. Cosmochim. Acta 50, 379–392.

TTT, 2009. Report for Treating Hanford LAW and WTP SW Simulants: Pilot Plant Flowsheet. April 2009. THOR Treatment Technologies, LLC, Denver, Colorado.

Vance, E.R., 2012. Ceramic waste forms. In: Konings, R.J.M. (Ed.), Comprehensive Nuclear Materials. Elsevier, Oxford, pp. 485–503.

Williams, B.D., Neeway, J.J., Valenta, M.M., Bowden, M.E., Amonette, J.E., Arey, B.W., Pierce, E.M., Brown, C.F., Qafoku, N.P., 2016. Mineral assemblage transformation of a metakaolin-based waste form after geopolymer encapsulation. Accepted to J. Nucl. Mater. http://dx.doi.org/10.1016/j.jnucmat.2015.12.023.

Xu, H., Navrotsky, A., Balmer, M.L., Su, Y., Bitten, E.R., 2001. Energetics of substituted pollucites along the $CsAlSi_2O_6$–$CsTiSi_2O_{6.5}$ join: a high-temperature calorimetric study. J. Am. Ceram. Soc. 84, 555–560.

Xu, H., Chavez, M.E., Mitchell, J.N., Garino, T.J., Schwarz, H.L., Rodriguez, M.A., Rademacher, D.X., Nenoff, T.M., 2015. Crystal structure and thermodynamic stability of Ba/Ti-substituted pollucites for radioactive Cs/Ba immobilization. J. Am. Ceram. Soc. 98, 2634–2640.

Zhang, Y., Zhang, Z., Thorogood, G., Vance, E.R., 2013. Pyrochlore based glass-ceramics for the immobilization of actinide-rich nuclear wastes: from concept to reality. J. Nucl. Mater. 432, 545–547.